Dyes and Pigments 89 (2011) 1–8

Contents lists available at ScienceDirect

Dyes and Pigments

journal homepage: www.elsevier.com/locate/dyepig

Synthesis, application and investigation of structure–thermal stability relationships of thermally stable water-soluble azo naphthalene dyes for LCD red color filters

Young Do Kim [a], Jung Hyun Cho [a], Chong Rae Park [a], Jae-Hong Choi [b], Chun Yoon [c], Jae Pil Kim [a,*]

[a] Department of Materials Science and Engineering, Seoul National University, Seoul 151-744, Republic of Korea
[b] Department of Textile System Engineering, Kyungpook National University, 1370 Sankyuk-dong, Buk-gu, Daegu 702-701, Republic of Korea
[c] Department of Chemistry, Sejong University, 98 Gunja-dong, Gwangjin-gu, Seoul 143-747, Republic of Korea

ARTICLE INFO

Article history:
Received 12 April 2010
Received in revised form
18 July 2010
Accepted 21 July 2010
Available online 10 August 2010

Keywords:
Azo dyes
LCD color filters
Dye-based color filters
Thermal stability
Intra-molecular interaction
Inter-molecular interaction

ABSTRACT

A series of structurally isomeric water-soluble azo naphthalene dyes were synthesized, and their thermal properties were examined by thermogravimetric analysis and differential scanning calorimetry. Dye-based color filters were also fabricated using the synthesized dyes. Transmittance (98.9%) at 650 nm and a wide color gamut (62.8%) were achieved using one of the color filters. All the prepared dyes had a degradation temperature above 280 °C, which varied with the dye structure. The degradation temperatures of the dyes were presumed to be related to the intra- and inter-molecular interactions of the structural isomers. From quantum mechanics calculations, their intra-molecular interactions were similar. However, the degradation temperatures generally increased in proportion to their density. According to the molecular mechanics calculations, the different structures induced changes in electrostatic attraction, steric hindrance and linearity of the dyes, which in turn caused changes in their molecular packing geometry, density and degradation temperature.

1. Introduction

Dyes have been traditionally used for the coloring of textiles. However, dyes are nowadays being employed in a range of high technology areas, such as display [1–5], energy [6–8], bio [9–11] and digital printing [12–14] industries. In particular, with the progress of display and digital printing industries, the necessity of using water-soluble dyes in these industries for the environmentally friendly organic solvent-free coloring process has increased. However, the weak thermal stability of water-soluble dyes is the main disadvantage in manufacturing dye-based LCD color filters (CFs) [15,16] and thermal type ink cartridges [17–20]. Nevertheless, there have been few systematic investigations of the thermal stability of water-soluble dyes for these purposes [21,22].

In this study, a range of water-soluble azo dyes with the same molecular weight, chemical formula and substituents were designed and synthesized. With these structurally isomeric dyes, dye-based color filters (D-CFs) were fabricated by spin-coating on transparent glass substrates. The absorbance, transmittance and chromaticity of the color filters were measured by UV–Vis spectrophotometry and colorimetry. In addition, their total energies and bond lengths for intra-molecular interactions, densities and molecular packing geometries for inter-molecular interactions were investigated to determine relationships between structure and thermal stability of the structurally isomeric dyes.

2. Experimental

2.1. Materials and instrumentation

5-Amino-1-naphthalenesulfonic acid (Laurent's acid), 5-amino-2-naphthalenesulfonic acid (1,6-Cleve's acid), 6-amino-1-naphthalenesulfonic acid (Dahl's acid), 6-amino-2-naphthalenesulfonic acid (Bronner's acid), and 2,4-dinitro-1-naphthol-7-sulfonic acid disodium salt (C.I. Acid Yellow 1) were purchased from TCI. 4-Hydroxy-2,7-naphthalenedisulfonic acid disodium salt (Rudolf Guercke acid) and 3-hydroxy-2,7-naphthalenedisulfonic acid disodium salt (R acid) were obtained from Sigma–Aldrich. All the above chemicals were used as received. All other reagents and solvents used were of reagent-grade quality. Transparent glass substrates were provided by Paul Marienfeld GmbH & Co. KG. Commercial acrylic binder of KGAP-823 was supplied by APEC Co., Ltd.

* Corresponding author. Tel.: +82 2 880 7187; fax: +82 2 880 7238.
E-mail address: jaepil@snu.ac.kr (J.P. Kim).

0143-7208/$ – see front matter © 2010 Elsevier Ltd. All rights reserved.
doi:10.1016/j.dyepig.2010.07.008

The ^{1}H nuclear magnetic resonance (NMR) spectra were recorded on a Bruker Avance 500 spectrometer at 500 MHz using DMSO-d_6 and TMS, as the solvent and internal standard, respectively. The mass spectra were recorded in fast atom bombardment (FAB) ionization mode using a JEOL JMS-AX505WA/HP 6890 Series II Gas Chromatography-Mass Spectrometer. The absorption and transmittance spectra were measured on a HP8452A spectrophotometer. Density data of the dyes was collected from a Micromeritics AccuPyc 1330 density analyzer. Thermogravimetric analysis (TGA, Thermogravimetric Analyzer 2050, TA Instruments) and Differential Scanning Calorimetry (DSC, Differential Scanning Calorimeter 2920, TA Instruments) were carried out under nitrogen at a heating rate of 10 K/min. Intra- and intermolecular interactions of the dye molecules were calculated by Dmol^3 and Discover embedded in a Materials Studio 4.3 (Accelrys, USA). The chromatic characteristics of the color filters were analyzed using an Otsuka Electronics LCF A2000 spectrometer. The thickness of the color filters was measured using a Nano System Nanoview E-1000.

2.2. Synthesis of dyes

Figs. 1 and 2 show the synthetic scheme of the dyes and their structures, respectively. All dyes were synthesized as previously described through direct diazotization [23,24] of 5-amino-1-naphthalenesulfonic acid (**1**), 5-amino-2-naphthalenesulfonic acid (**2**), 6-amino-1-naphthalenesulfonic acid (**3**) and 6-amino-2-naphthalenesulfonic acid (**4**), followed by the coupling of the diazonium salts with 4-hydroxy-2,7-naphthalenedisulfonic acid disodium salt (**a**) and 3-hydroxy-2,7-naphthalenedisulfonic acid disodium salt (**b**) in an alkaline medium [25]. After adding sodium chloride to the solution, the precipitate formed was filtered, washed with ethanol and dried in a vacuum oven at 40 °C. The crude product was heated in ethanol for 2 h under reflux, hot filtered, washed with hot ethanol and then dried in a vacuum oven. To remove the remaining sodium chloride, 2 g of the product was dissolved in 80 ml of N,N-dimethylmethanamide. The mixture solution was then poured into 600 ml of diethyl ether, and the precipitate was filtered and dried at 40 °C under vacuum. The purity of the prepared dyes was confirmed by thin layer chromatography using isopropyl alcohol/acetone/ammonia (1:2:1) as the mobile phase. Table 1 lists the yield, absorption maxima (λ_{max}), molar extinction coefficients (ε_{max}), ^{1}H NMR and mass data of the synthesized dyes.

2.3. Preparation of dye-based inks

1 wt% of aqueous red ink was composed of the synthesized dyes (10.0 mg), distilled water (0.5 ml), and KGAP-823 (0.5 ml) as a binder based on acrylate. 5 wt% of aqueous red ink was composed of dye **4a** (30.0 mg), C.I. Acid Yellow 1 (20 mg), distilled water (0.5 ml), and KGAP-823 (0.5 ml). 10 wt% of aqueous red ink was composed of dye **4a** (60.0 mg), C.I. Acid Yellow 1 (40 mg), distilled water (0.5 ml), and KGAP-823 (0.5 ml).

2.4. Fabrication of dye-based color filters

The dye-based inks were coated onto a transparent glass substrate using a MIDAS System SPIN-1200D spin coater. The coating speed was kept for 10 s at 300 rpm. The speed was increased to 700 rpm and kept at that rate for 50 s. The wet dye-coated color filters were baked at 150 °C for 1 h. All spin coated dye-based color filters were 1.7 μm thick.

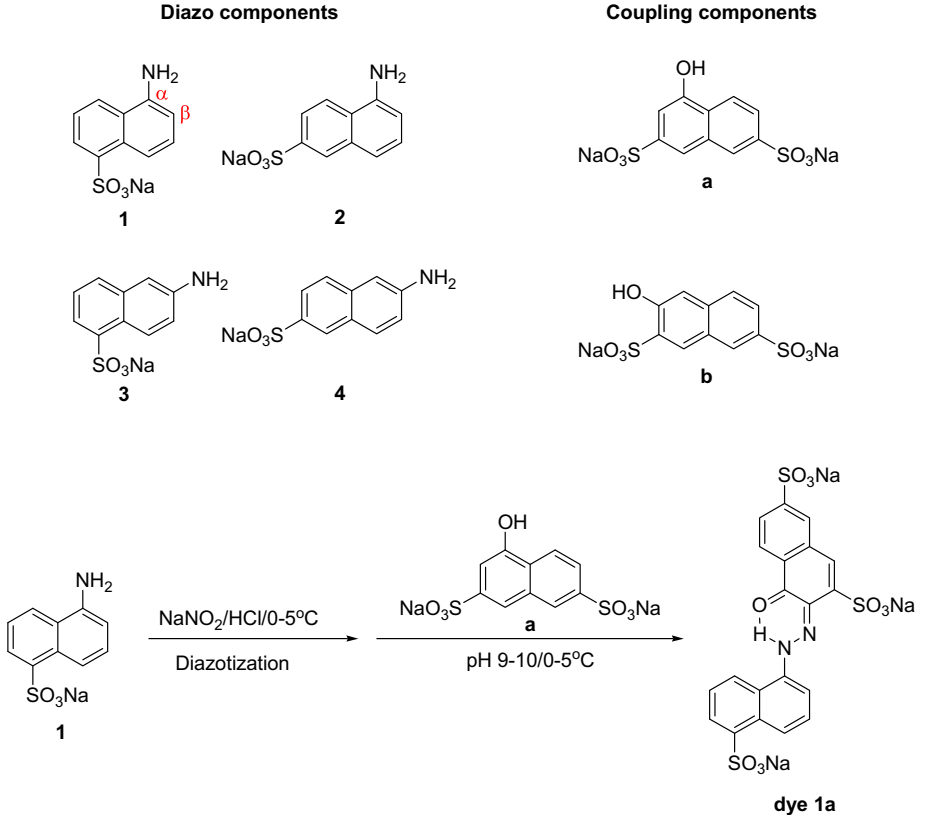

Fig. 1. Reagents and representative synthetic scheme for the dyes studied.

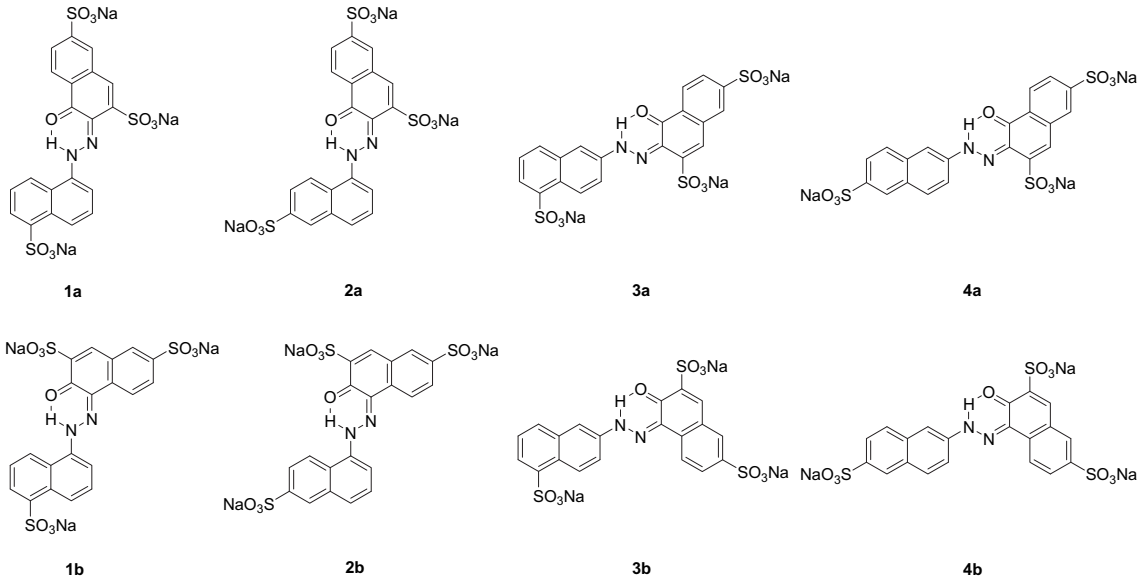

Fig. 2. Structures of the prepared dyes.

2.5. Quantum mechanics (QM) and molecular mechanics (MM) calculation

To evaluate the intra-molecular interaction of the dye molecules, density functional theory (DFT) calculations were performed using the local density approximation (LDA) functional [26]. A double numerical plus d-functions (DND) was adopted as the basis set, which is embedded in the Dmo1[3] (Materials Studio, Accelrys, USA) [27]. The orbital cut-off distance and energy convergence were set to 4.5 Å and 0.026 kJ/mol respectively.

Molecular mechanics (MM) calculations were used to calculate the optimized molecular packing geometries of the prepared dyes. The DREIDING ForceField (FF) [28] was adopted to optimize the structure of dyes, which included a 6-membered ring induced by H-bonding between −C═O and H−N−N− in the hydrazone form, because this FF is known to be moderately accurate for the optimization and calculation of the geometry, conformational energy, inter-molecular binding energy and crystal packing of organic molecules. The qEq charge equilibrium method [29], which is applicable to the sodium sulfonate ionic bond, was also used to assign the atomic charge of the dyes.

3. Results and discussion

3.1. Synthesis and spectral properties of dyes

The diazo-components of the dyes were coupled to the *ortho*-position of the hydroxyl group of the coupling components to make the dyes water-soluble. 2-Azo-1-naphthol derivatives exist mainly in hydrazone form via intra-molecular hydrogen bonds, which results in the linearity and coplanar conformation of the dyes (Fig. 2) [30]. The proton peaks involved in intra-molecular hydrogen bonding appeared at a much lower field in the ^{1}H NMR spectrum (17.4–16.3 ppm for dyes of **1a**–**4b**) than the normal proton peak of the hydroxyl group [31].

Table 1 lists the spectral properties of the prepared dyes. As shown in the table, dyes coupled at the α-position of the diazo-component were bathochromic compared to those coupled at the β-position. On the other hand, the molar extinction coefficients of dyes **1a**–**4a** were higher than those of dyes **1b**–**4b**.

3.2. Spectral and chromatic properties of dye-based color filters

To apply a dye to LCD red color filters, the dye needs to have a sharp absorption spectrum near 500 nm and thermal stability

Table 1
Yields, spectral properties, ^{1}H NMR and mass data of the prepared dyes.

Dye	Yield (%)	λ_{max}[a] (nm)	ε_{max}[a] ($1\ mol^{-1}\ cm^{-1}$)	^{1}H NMR (ppm, DMSO-d_6)	Mass (m/z)
1a	68	518	21,000	7.64 (s, 1H), 7.70 (t, 1H), 7.74 (t, 1H), 7.77 (d, 1H), 7.79 (s, 1H), 8.10 (d, 1H), 8.24 (d, 2H), 8.37 (d, 1H), 8.86 (d, 1H), 17.44 (s, 1H, OH)	605 (100%, $[M+H]^+$)
1b	71	518	17,000	7.70 (t, 1H), 7.73 (t, 1H), 7.84 (s, 1H), 7.95 (s, 1H), 7.98 (d, 1H), 8.12 (d, 1H), 8.31 (d, 1H), 8.45 (d, 1H), 8.64 (d, 1H), 8.92 (d, 1H), 17.26 (s, 1H, OH)	605 (100%, $[M+H]^+$)
2a	72	518	26,000	7.63 (s, 1H), 7.70 (t, 1H), 7.77 (d, 1H), 7.93 (s, 1H), 7.98 (d, 1H), 7.98 (d, 1H), 8.23 (d, 1H), 8.25 (d, 1H), 8.29 (s, 1H), 8.37 (d, 1H), 17.30 (s, 1H, OH)	605 (100%, $[M+H]^+$)
2b	57	518	22,000	7.73 (t, 1H), 7.84 (d, 1H), 7.95 (s, 1H), 7.96 (d, 1H), 8.01 (s, 1H), 8.03 (d, 1H), 8.29 (s, 1H), 8.33 (d, 1H), 8.39 (d, 1H), 8.60 (d, 1H), 17.30 (s, 1H, OH)	605 (100%, $[M+H]^+$)
3a	69	502	34,000	7.50 (t, 1H), 7.60 (s, 1H), 7.86 (d, 1H), 7.92 (s, 1H), 7.92 (d, 2H), 8.12 (d, 1H), 8.23 (s, 1H), 8.29 (d, 1H), 8.92 (d, 1H), 19.38 (s, 1H, OH)	605 (100%, $[M+H]^+$)
3b	62	502	24,000	7.48 (t, 1H), 7.71 (s, 1H), 7.92 (d, 1H), 7.95 (s, 1H), 7.98 (d, 1H), 8.06 (d, 1H), 8.14 (d, 1H), 8.33 (s, 1H), 8.60 (d, 1H), 8.94 (d, 1H), 16.59 (s, 1H, OH)	605 (100%, $[M+H]^+$)
4a	60	502	36,000	7.59 (s, 1H), 7.76 (s, 1H), 7.76 (d, 1H), 7.89 (d, 1H), 7.91 (s, 1H), 8.11 (d, 1H), 8.19 (d, 2H), 8.19 (s, 1H), 8.28 (d, 1H), 16.34 (s, 1H, OH)	605 (100%, $[M+H]^+$)
4b	63	502	26,000	7.86 (d, 1H), 7.95 (s, 1H), 8.00 (s, 1H), 8.02 (d, 1H), 8.11 (d, 1H), 8.19 (d, 1H), 8.22 (s, 1H), 8.32 (s, 1H), 8.33 (d, 1H), 8.54 (d, 1H), 16.64 (s, 1H, OH)	605 (100%, $[M+H]^+$)

[a] Measured in H_2O.

at above 250 °C [15,16]. Fig. 3(a) shows the absorption spectra of the fabricated color filters with 1 wt% of the prepared dyes. All the prepared red color filters had absorption maxima between 502 and 520 nm, and their molar extinction coefficients varied with the dye structure. The color filters with the **3a**, **3b**, **4a** and **4b** dyes had absorption maxima between 502 nm and 504 nm, and the color filters had high transmittances above 600 nm, as shown in Fig. 3(b). In particular, since dye **4a** has the highest molar extinction coefficients, the color filter using dye **4a** could have the lowest transmittance at 500 nm. However, dye **4a** had undesirable transmittance at 400–500 nm. Nevertheless, an excellent red spectrum could be obtained by adding C.I. Acid Yellow 1, which could cut down transmittance at 400–500 nm.

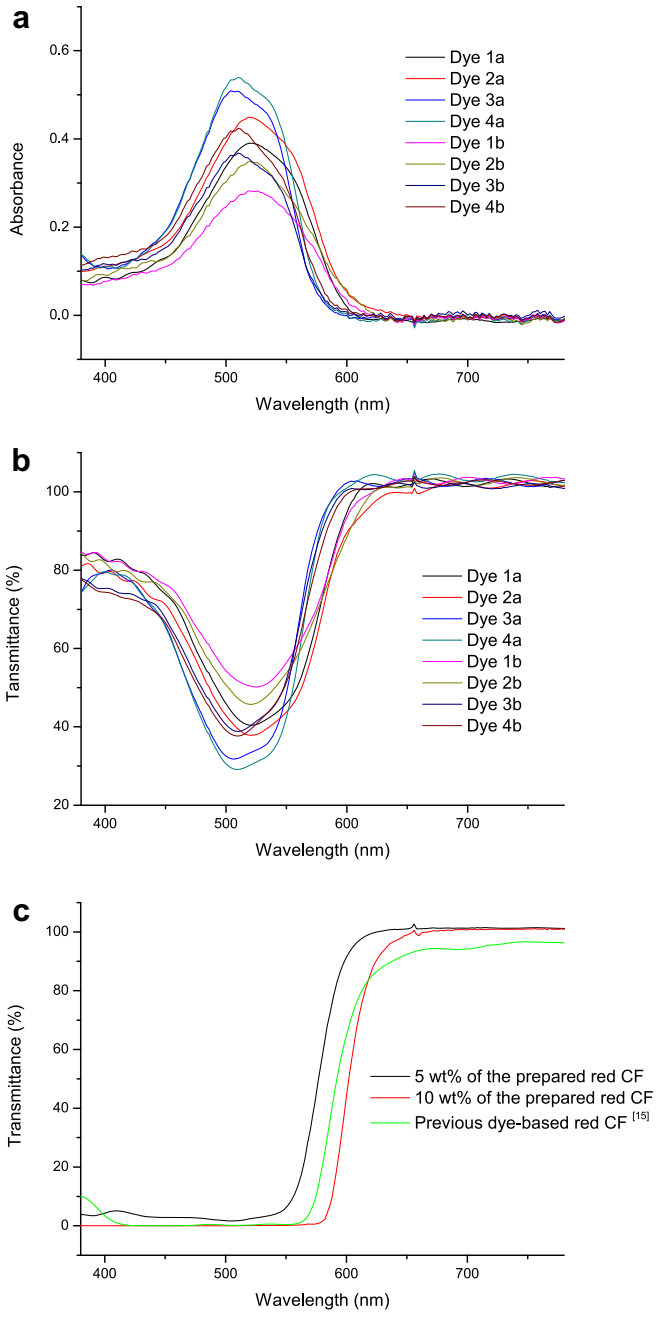

Fig. 3. Spectral properties of the prepared color filters. (a) Absorption spectra of the fabricated color filters with 1 wt% of the prepared dyes. (b) Transmittance spectra of the fabricated color filters with 1 wt% of the prepared dyes. (c) Transmittance spectra of the color-compensated red color filters with yellow dyes.

Fig. 3(c) shows the transmittance spectra of the color-compensated red color filters. The red D-CF of 5 wt% and 10 wt% dye content showed 100% and 98.9% transmittance at 650 nm respectively. These values were 8.23% and 7.03% higher than 92.4% of our previous manufactured red D-CF [15].

This high transmittance of the dye **4a**-based CF might be due to following three reasons. (1) The prepared water-soluble azo dyes have three sodium sulfonate water-solubilizing groups, while the water-soluble perylene dye has two sodium sulfonate groups [15]. Therefore, the azo dyes could have higher solubility in water and compatibility for the hydrophilic acrylic binder than those of the perylene dye, which resulted in the low aggregation of dye molecules in the water-based ink. Low aggregation leads to low light scattering, which could increase the transmittance of the prepared D-CFs. (2) Dye **4a** has a higher molar extinction coefficient than the perylene dye used in previous red D-CF [15]. Therefore, the red D-CF with dye **4a** could have a lower dye content, which results in higher transmittance than the previous red D-CF. (3) The C.I. Acid Yellow 1 (2,4-dinitro-1-naphthol-7-sulfonic acid disodium salt) color compensating dye can be dissolved easily in the media (water) and has higher compatibility with the water-soluble binder than the Solvent Yellow 146 (metal free mono azo dye) color compensating dye for the previous red D-CF due to its sulfonic acid group [15]. Therefore, the higher solubility in water and compatibility with the binder of Acid Yellow 1 may result in less aggregation in the water-based ink, which could enhance the transmittance of the prepared red D-CF.

In addition, as shown in Fig. 4, the D-CF with dye **4a** and Acid Yellow 1 had wider color gamut of 62.8% than the previous D-CF, which had a value of 57.3%, even though the CF had lower dye content than the previous D-CF (10 wt% vs. 15 wt%) [15]. This could be due to the high molar extinction coefficient of dye **4a**.

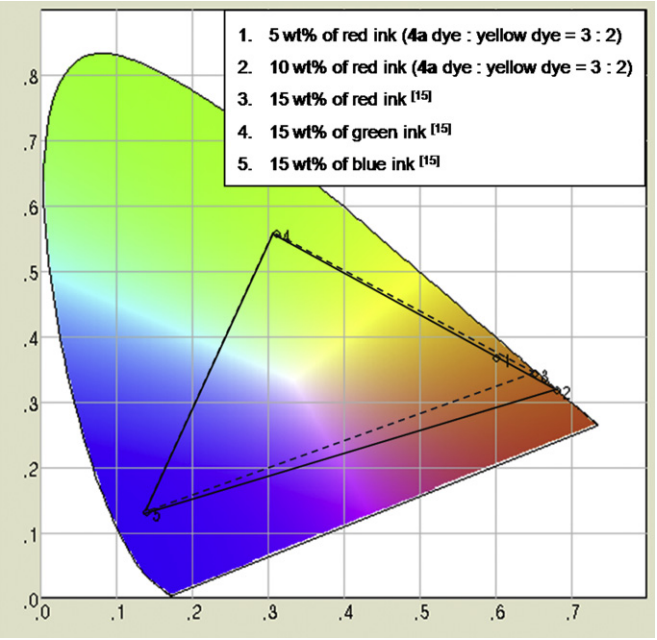

Fig. 4. CIE 1931 chromaticity diagram of the prepared dye-based color filter (solid line) and previous dye-based color filter (dashed line).

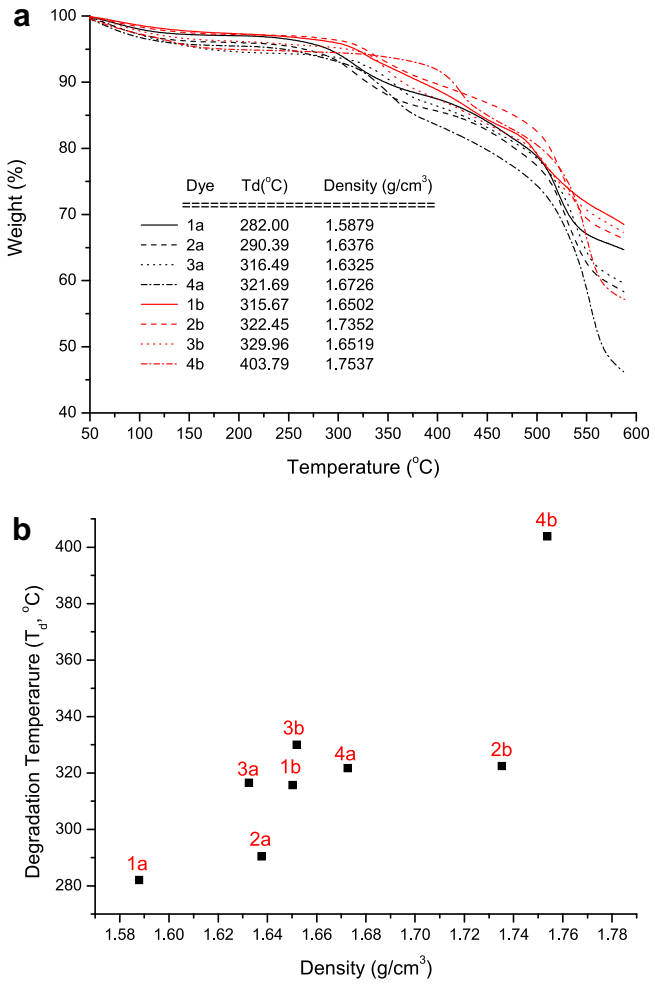

Fig. 5. TGA and density data. (a) TGA curves, degradation temperatures and densities of the prepared dyes. (b) Relationship between the degradation temperature and density. (The weight loss up to 150 °C is due to the evaporation of H_2O and DMF.)

3.3. Structure–thermal stability relationships of dyes

All the prepared dyes showed degradation temperatures of above 280 °C (Fig. 5). However, the degradation temperatures (T_d) varied according to the structure of the prepared dyes. This structural difference in the dyes will result in a change in the intra- and inter-molecular interactions of the dyes. Therefore, it is only logical to assume that the thermal stability of the prepared dyes is related to the intra- and inter-molecular interactions between the dye molecules. The effect of the intra- and inter-molecular interactions resulting from the structural difference in the dyes on their thermal stability is discussed.

3.3.1. Intra-molecular interaction of dyes

In general, hydroxyl azo dyes can cause azo–hydrazone tautomerism, and dyes with the hydrazone form and intra-molecular hydrogen bonding have higher thermal stability than those with the azo forms [30]. Therefore, when a dye shows tautomerism, the energy difference between the azo and hydrazone form could affect its thermal equilibrium. Table 2 shows the total energies of the prepared dyes using QM calculations. The energy differences between the hydrazone and azo forms ranged from 82 to 105 kJ/mol, as shown in the 4th column of Table 2. These correspond to the additional strength of the intra-molecular N–H···O hydrogen bond with a 6-membered ring structure in the hydrazone form compared to that in the azo form. Since the energy at room temperature (300 K) corresponds to 2.5 kJ/mol, most of the synthesized dyes should exist in the hydrazone forms at room temperature, which was confirmed by ^{1}H NMR, as shown in Table 1.

The change in the total energies of the dye molecules can also be induced from the difference in the intra-molecular hydrogen bond length or azo bond length. The 2nd column of Table 3 shows that the hydrogen bond lengths of the prepared dyes were 1.516–1.535 Å, which are shorter than the general hydrogen bond length of 1.7 Å. This is due to the resonance stabilization effect of the hydrazone form with a 6-membered ring structure [32]. The 3rd and the 4th columns of Table 3 show the azo bond lengths of the prepared dyes. The azo form has bond lengths of 1.259–1.265 Å, whereas the bond lengths of the hydrazone are 1.288–1.293 Å. However, since the variation in hydrogen bond length and azo bond length was quite small (<0.019 Å), it was difficult to find a meaningful relationship between the total energy and bond lengths of the dye molecules.

The 5th column of Table 2 shows the differences in the total energies of the **a** and **b** dyes. When the dyes in the hydrazone form with the same diazo-compound were compared, the total energies of dyes **1b**–**4b** were 42–50 kJ/mol lower than those of dyes **1a**–**4a**. According to QM calculations, two of the three oxygen atoms in SO_3^- interacted with Na^+ as shown in Fig. 6. On the other hand, dyes **1b**–**4b** had one $SO_3^-Na^+$ ionic pair at the *ortho*-position of the carbonyl group. Consequently, its specific sodium cation $(Na(II)^+)$ could make a multi-ionic interaction with the oxygen atom (O(II)) of the nearby carbonyl group as well as those in SO_3^-. These multi-ionic interactions of the sodium cation could strengthen the intra-molecular electrostatic attraction of dyes **1b**–**4b**, which results in dyes **1b**–**4b** having a lower total energy than dyes **1a**–**4a**.

Table 2
Total energies of the prepared dyes using QM calculations (unit = kJ/mol).

Dye	Total energy[a]					
	Azo form	Hydrazone form	Difference of energy between azo and hydrazone form	For hydrazone form		
				Difference of **a** and **b** dyes	Dyes without $SO_3^-Na^+$	Difference of **a** and **b** dyes without $SO_3^-Na^+$
1a	−8,643,783	−8,643,883	100	42	−2,486,021	4
1b	−8,643,843	−8,643,925	82		−2,486,017	
2a	−8,643,775	−8,643,880	105	45	−2,486,021	4
2b	−8,643,841	−8,643,925	84		−2,486,017	
3a	−8,643,780	−8,643,885	105	50	−2,486,022	3
3b	−8,643,846	−8,643,935	89		−2,486,019	
4a	−8,643,791	−8,643,888	97	42	−2,486,022	3
4b	−8,643,836	−8,643,930	94		−2,486,019	

[a] Energy of the geometrically optimized dye structure using DFT calculations.

Table 3
Bond lengths of the prepared dyes geometrically optimized with QM calculation.

Dye	Bond length (Å)				
	Hydrogen bonding of O(II)[b]···H	Azo bonding		Ionic bonding	
		Azo form (−N=N−)	Hydrazone form (−N−N=)	O(I)[a]···Na(I)[c]	O(I)[a]···Na(I)[c], O(II)[b]···Na(II)[d]
1a	1.517	1.259	1.288	2.184	–
1b	1.531	1.264	1.291	2.189	2.235, 2.241
2a	1.517	1.262	1.288	2.183	–
2b	1.529	1.263	1.291	2.190	2.232, 2.255
3a	1.517	1.259	1.288	2.182	–
3b	1.527	1.264	1.289	2.190	2.278, 2.239
4a	1.516	1.260	1.288	2.184	–
4b	1.535	1.265	1.293	2.190	2.228, 2.251

[a] O(I) is the oxygen of the sodium sulfonate salt.
[b] O(II) is the oxygen of the carbonyl groups in hydrazone formed azo dyes.
[c] Na(I) is the sodium of the general sodium sulfonate salt.
[d] Na(II) is the sodium of the specific sodium sulfonate salt which is located at the *ortho*-position to the carbonyl group in the hydrazone formed azo dyes.

However, in dyes **1b**–**4b** as shown in Fig. 3, with the additional Na(II)···O(II)=C attraction, the C=O(II)···H–N hydrogen bonds were 0.01–0.02 Å longer than those of dyes **1**–**4a** (the 2nd column of Table 3). Hence, the multi-ionic interaction of the sodium cation stabilized the total energy of the dye molecule, even though it decreased the strength of the intra-molecular hydrogen bond. An examination of the total energy of the hydroxyl azo naphthalene dyes without ionic sodium sulfonate functional groups revealed all the dyes to have extremely small energy differences (~4 kJ/mol), as shown in the 7th column of Table 2 (here, dyes **1a** and **2a**, **1b** and **2b**, **3a** and **4a**, and **3b** and **4b** have identical molecular structures). Therefore, the Na(II)···O(II)=C electrostatic attraction in the dye molecules lowered the total energies of dyes **1b**–**4b**.

3.3.2. Inter-molecular interaction of dyes

Fig. 5(a) shows the TGA curves and densities of the prepared dyes. The dyes decomposed at different temperatures, even though they had the same molecular weight and covalent bonding, such as C–N, C–O, C–S, N–N and N–H, etc. However, as stated in session 3.3.1., the differences in their total energies for the hydrazone form were as small as below 55 kJ/mol. Judging from the above results, the change in the degradation temperatures of the dyes is believed to be related more to their inter-molecular interactions. DSC analysis was conducted to examine the inter-molecular interactions of the dyes, but their melting peaks could not be confirmed. This is different from the general melting and decomposition behavior of dyes, and the results of a study of the decomposition behavior of the prepared dyes will be reported in a separate paper.

Since a dye with a stronger inter-molecular interaction could have a higher density than the others, the inter-molecular interactions of the prepared dyes of structural isomers could be examined by comparing their densities. Fig. 5(b) shows the relationship between the degradation temperatures and densities of the prepared dyes. The degradation temperatures generally increased with increasing density. Therefore, the thermal stability of the prepared dyes was related to their density.

The density of a dye is related to its molecular packing geometry, which could be evaluated by MM calculations. Fig. 7 shows the representative packing structure of dye **4b**. The dye molecules are aggregated three-dimensionally via strong electrostatic attractions between the three pairs of sodium sulfonate groups. Due to this aggregation behavior, all the prepared dyes had high thermal stability (T_d > 280 °C). This optimization of the molecular packing geometry can be affected by the change in electrostatic attraction, steric hindrance and linearity of dye molecules.

3.3.2.1. Effect of electrostatic attraction. Dyes **1b**–**4b** (red lines) generally show higher degradation temperatures and densities

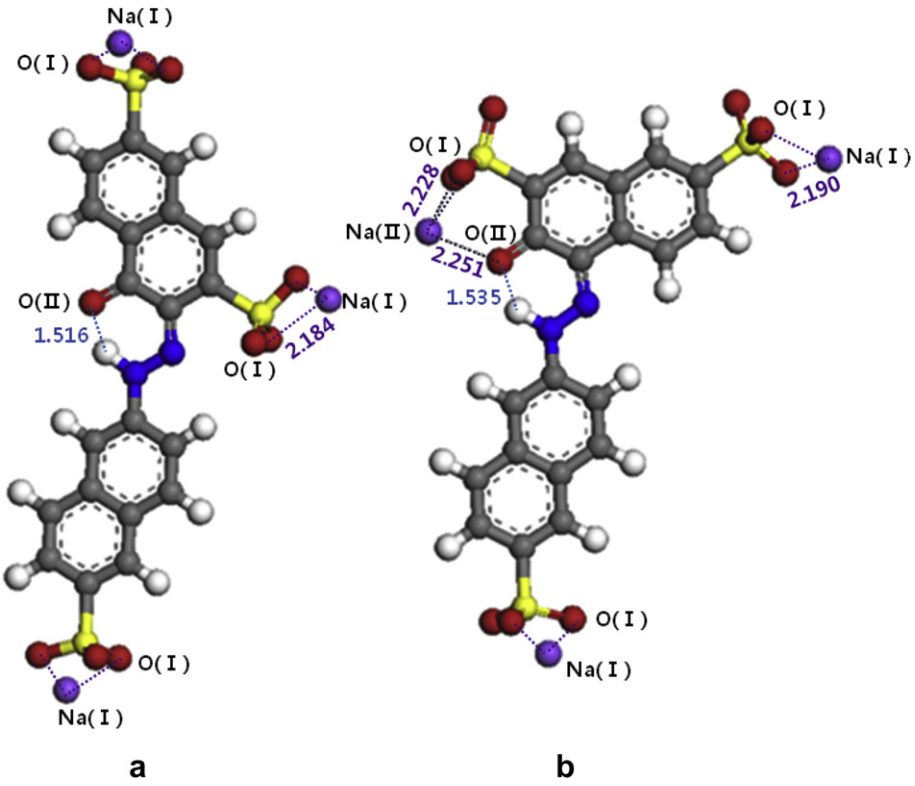

Fig. 6. Optimized molecular structure of dyes **4a** (a) and **4b** (b) by QM calculations (unit = Å).

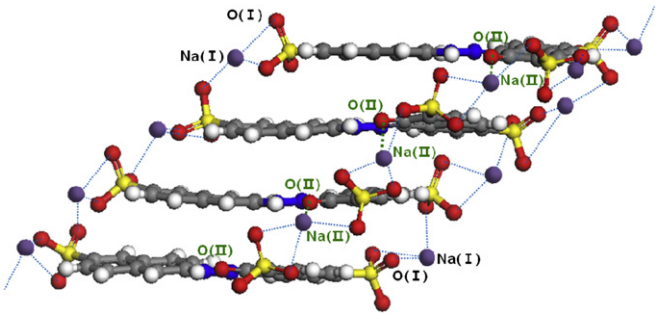

Fig. 7. Representative packing structure of dye **4b** by MM calculation.

than those of dyes **1a**–**4a** (black lines), as shown in Fig. 5(a). (For interpretation of the references to colour in the text, the reader is referred to the web version of this article.) In the case of dyes **1a**–**4a**, all sodium sulfonate ($SO_3^-Na^+$) groups of the dyes make the general salt form by ionic interaction. However, in dyes **1b**–**4b**, there is a specific sodium sulfonate group that is located at the *ortho*-position to the carbonyl group in the hydrazone form. This can make an additional electrostatic attraction with O(II) of the adjacent carbonyl group (Fig. 6). In addition, $Na(II)^+$ can make a multi-ionic interaction with C═O(II) and $SO(I)_3$ of the neighboring dye molecules, which can strengthen the inter-molecular electrostatic attractions as well as the intra-molecular electrostatic attractions of the dyes, as shown in Fig. 7 and the 5th column of Table 2. Consequently, due to the more effective packing of dyes **1b**–**4b** than that of dyes **1a**–**4a**, the densities of dyes **1b**–**4b** can be increased, resulting in an increase in their degradation temperature.

3.3.2.2. Effect of steric hindrance. In order for the prepared dyes to have dense packing geometry, the strength of the inter-molecular electrostatic attractions between the three pairs of sodium sulfonate groups should be similar and there should be no torsion in the dye molecule. Dyes **2b** and **4b** had higher degradation temperatures than dyes **1b** and **3b**. These results might be caused by steric hindrance of the pendant sulfonate group of the diazo-component. Fig. 8 shows the optimized packing geometries of dyes **1b**–**4b** according to MM calculations. In the case of dyes **2b** and **4b**, the adjacent dye molecules were packed parallel due to the well-balanced electrostatic attractions between the three pairs of sodium sulfonate groups. On the other hand, in dyes **1b** and **3b**, the electron rich sodium sulfonate group in the diazo-component pushes the electron rich aromatic ring of the adjacent dye molecule and distorts the parallel molecular packing structure. Therefore, dyes **2b** and **4b** could have a more compact molecular packing structure with higher density, which would result in higher degradation temperatures than dyes **1b** and **3b**.

3.3.2.3. Effect of linearity. The linearity of the dye molecules studied was affected by the position of the amine group in the diazo-component. The dye coupled at the β-position of the diazo-component had a more linear structure than the dye coupled at the α-position of the diazo-component [32,33]. The degradation temperatures of dyes **4b** and **3b** were higher than those of dyes **2b** and **1b** (Fig. 5). As shown in Figs. 1 and 2, dyes **4b** and **3b** have diazo-components with amine groups substituted at the β-position of the naphthalene ring, which results in a more linear structure. Therefore, dyes **4b** and **3b** may have denser packing structures which could increase the degradation temperature compared to dyes **2b** and **1b**.

4. Conclusion

Eight structurally isomeric water-soluble azo dyes were synthesized and their thermal stabilities were examined. All the prepared dyes showed high degradation temperatures (above 280 °C), while they did not have clear melting temperatures. This might be caused by the aggregation behavior by the strong inter-molecular electrostatic attractions.

Red color filters with the prepared dyes had absorption maxima between 500 nm and 520 nm. The optimal color filter was fabricated with dye **4a** and commercial yellow dye, which showed 98.9% transmittance and a 62.8% color gamut. Its transmittance and color gamut were improved by 7.03% and 9.6%, respectively, compared to the previous dye-based color filter.

The degradation temperatures of the prepared dyes varied according to their structure, and the structure–thermal stability relationships were examined using the prepared structurally isomeric dyes. The prepared dyes had similar intra-molecular interactions but their thermal stability increased in proportion to their inter-molecular interactions, which could be represented by their densities. MM calculations of the molecular packing structure of the prepared dyes suggested that the electrostatic attraction,

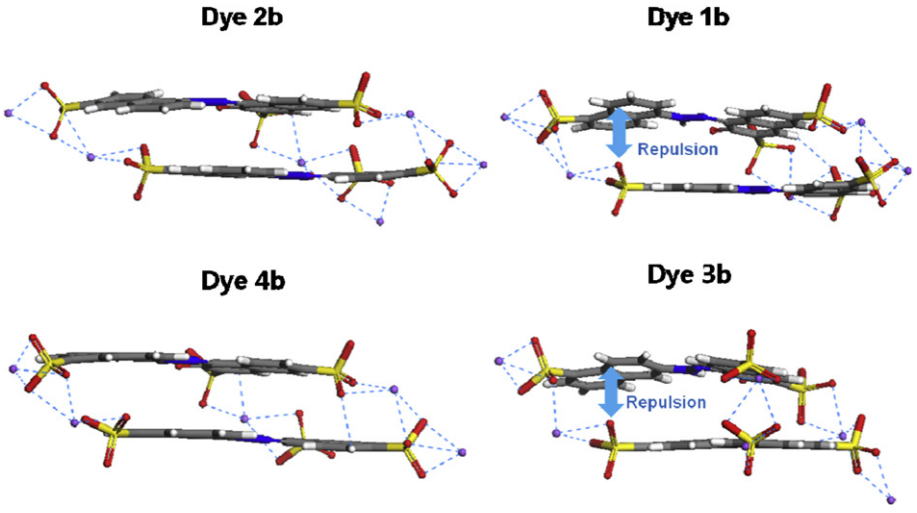

Fig. 8. Optimized packing geometries of the dyes **1b**–**4b** by MM calculations.

steric hindrance and linearity of the dyes could be changed by the position of the azo linkage and sodium sulfonate groups. When the dyes had multi-ionic interactions and linear structures, they could have dense molecular packing structures. On the other hand, steric hindrance between the neighboring dye molecules disturbed the effective molecular packing. The results of MM calculations of the molecular packing corresponded to those of density analysis. In conclusion, for application of the dyes in LCD color filters, dyes with more compact packing structures may have higher density values and degradation temperatures.

Acknowledgements

This work was supported by a grant from the Fundamental R&D Program for Core Technology of Materials funded by the Ministry of Knowledge Economy, Republic of Korea.

References

[1] Hu Z, Xue M, Zhang Q, Sheng Q, Liu Y. Nanocolorants: a novel class of colorants, the preparation and performance characterization. Dyes and Pigments 2008;76:173–8.
[2] Koo HS, Chen M, Pan PC, Chou LT, Wu FM, Chang SJ, et al. Fabrication and chromatic characteristics of the greenish LCD colour-filter layer with nanoparticle ink using inkjet printing technique. Displays 2006;27:124–9.
[3] Sabnis RW. Color filter technology for liquid crystal displays. Displays 1999;20:119–29.
[4] Sugiura T. Dyed color filters for liquid-crystal displays. Journal of the SID 1993;1:177–80.
[5] Tsuda K. Color filters for LCDs. Displays 1993;14:115–24.
[6] O'Regan B, Grätzel M. A low-cost, high-efficiency solar cell based on dye-sensitized colloidal TiO_2 films. Nature 1991;353:737–40.
[7] Bai Y, Cao Y, Zhang J, Wang M, Li R, Wang P, et al. High-performance dye-sensitized solar cells based on solvent-free electrolytes produced from eutectic melts. Nature Materials 2008;7:626–30.
[8] Kim S, Lee JK, Kang SO, Ko J, Yum JH, Fantacci S, et al. Molecular engineering of organic sensitizers for solar cell applications. Journal of the American Chemical Society 2006;128:16701–7.
[9] Dolmans DE, Fukumura D, Jain RK. Photodynamic therapy for cancer. Nature Reviews Cancer 2003;3:380–7.
[10] Zhou L, Zhou JH, Dong C, Ma F, Wei SH, Shen J. Water-soluble hypocrellin a nanoparticles as a photodynamic therapy delivery system. Dyes and Pigments 2009;82:90–4.
[11] Gorman SA, Bell AL, Griffiths J, Roberts D, Brown SB. The synthesis and properties of unsymmetrical 3,7-diaminophenothiazin-5-ium iodide salts: potential photosensitisers for photodynamic therapy. Dyes and Pigments 2006;71:153–60.
[12] Calvert P. Inkjet printing for materials and devices. Chemistry of Materials 2001;13:3299–305.
[13] Yang Y, Naarani V. Improvement of the lightfastness of reactive inkjet printed cotton. Dyes and Pigments 2007;74:154–60.
[14] Hladnik A, Muck T. Characterization of pigments in coating formulations for high-end ink-jet papers. Dyes and Pigments 2002;54:253–63.
[15] Kim YD, Kim JP, Kwon OS, Cho IH. The synthesis and application of thermally stable dyes for ink-jet printed LCD color filters. Dyes and Pigments 2009;81:45–52.
[16] Chang CJ, Chang SJ, Shin KC, Pan FL. Improving mechanical properties and chemical resistance of ink-jet printer color filter by using diblock polymeric dispersants. Journal of Polymer Science, Part B: Polymer Physics 2005; 43:3337–53.
[17] Ohya H, Morimoto H. Water based ink composition and image forming method. US 2001/0023652 A1.
[18] Ishizuka T, Hokazono H, Yamanouchi J. Color composition, ink for ink-jet recording and ink-jet recording method. US 6670410 B2.
[19] Koga N, Goto K, Kobayashi N, Aoyama M, Higashiyama S, Fujioka M. Water base ink for ink-jet recording. US 6648463 B2.
[20] Oki Y, Kitamura K, Aoyama T, Uotani N, Takahashi H, Ito Y. Aqueous ink. US 2002/0050226 A1.
[21] Lee JJ, Lee WJ, Choi JH, Kim JP. Synthesis and application of temporarily solubilised azo disperse dyes containing β-sulphatoethylsulphonyl group. Dyes and Pigments 2005;65:75–81.
[22] Koh J, Kim JD, Kim JP. Synthesis and application of a temporarily solubilised alkali-clearable azo disperse dye and analysis of its conversion and hydrolysis behavior. Dyes and Pigments 2003;56:17–26.
[23] Zollinger H. Diazo chemistry I: aromatic and heteroaromatic. New York: VCH; 1994. p. 11–20.
[24] Fierz-David HE, Blangey L. Fundamental processes of dye chemistry. New York: Interscience; 1949. p. 241–9.
[25] Fierz-David HE, Blangey L. Fundamental processes of dye chemistry. New York: Interscience; 1949. p. 262–9.
[26] Perdew JP, Wang Y. Accurate and simple analytic representation of the electron-gas correlation energy. Physical Review B 1992;45(23):13244–9.
[27] Delley B. An all-electron numerical method for solving the local density functional for polyatomic molecules. Journal of Chemical Physics 1990; 92:508–17.
[28] Mayo SL, Olafson BD, Goddard WA. Dreiding – a generic force field for molecular simulations. Journal of Physical Chemistry 1990;94(26):8897–909.
[29] Rappe AK, Goddard WA. Charge equilibration for molecular dynamics simulations. Journal of Physical Chemistry 1991;95(8):3358–63.
[30] Gordon PF, Gregory P. Organic chemistry in colour. Berlin: Springer-Verlag; 1983. p. 96–108.
[31] Skrabal P, Zollinger H. Mechanism of azo coupling reactions: part XXXV. pH-dependence and ortho/para ratio in coupling reactions of amino-hydroxynaphthalenesulfonic acids. Dyes and Pigments 1988;9:201–7.
[32] Song DH, Kim JP. Effect of transition moments and orientational behavior of dichroic dyes on the optical anisotropy of poly(vinyl alcohol) polarizing films. Dyes and Pigments 2009;80:219–25.
[33] Song DH, Yoo HY, Kim JP. Synthesis of stilbene-based azo dyes and application for dichroic materials in poly(vinyl alcohol) polarizing films. Dyes and Pigments 2007;75:727–31.